SUPPLEMENTAL DATA

Clonal germinal center B cells function as a niche for T-cell lymphoma

Manabu Fujisawa[1], Tran B. Nguyen[1], Yoshiaki Abe[2], Yasuhito Suehara[3], Kota Fukumoto[1,3], Sakurako Suma[2], Kenichi Makishima[2], Chihiro Kaneko[1], Yen T. M. Nguyen[1], Kensuke Usuki[4], Kentaro Narita[5], Kosei Matsue[5], Naoya Nakamura[6], Shumpei Ishikawa[7], Fumihito Miura[8], Takashi Ito[8], Ayako Suzuki[9], Yutaka Suzuki[9], Seiya Mizuno[10], Satoru Takahashi[10], Shigeru Chiba[1,3*] and Mamiko Sakata-Yanagimoto[1,3,11*]

[1]*Department of Hematology, Faculty of Medicine, University of Tsukuba.*

[2]*Department of Hematology, Graduate School of Comprehensive Human Sciences, University of Tsukuba.*

[3]*Department of Hematology, University of Tsukuba Hospital.*

[4]*Department of Hematology, NTT Medical Center Tokyo.*

[5]*Division of Hematology/Oncology, Department of Internal Medicine, Kameda Medical Center.*

[6]*Department of Pathology, Tokai University School of Medicine.*

[7]*Department of Preventive Medicine, Graduate School of Medicine, The University of Tokyo.*

[8]*Department of Biochemistry, Kyushu University Graduate School of Medical Sciences.*

[9]*Department of Computational Biology and Medical Sciences, Graduate School of Frontier Sciences, The University of Tokyo.*

[10]*Laboratory Animal Resource Center in Transborder Medical Research Center, Faculty of Medicine, University of Tsukuba.*

[11]*Division of Advanced Hemato-Oncology, Transborder Medical Research Center, University of Tsukuba.*

* These authors contributed equally to this work

Correspondence: sakatama@md.tsukuba.ac.jp (M.S.-Y.), schiba-t@md.tsukuba.ac.jp (S.C.)

Department of Hematology, Faculty of Medicine, University of Tsukuba

1-1-1 Tennodai, Tsukuba, Ibaraki 305-8575, Japan

Tel: +81-29-853-3127; Fax: +81-29-853-8079

Supplemental Notes

Supplemental Note1

Related to "Clonal expansion of *Tet2*-deficient GCB cells sorted from tumor-bearing MxTR"

To explore the biological significance of core histone mutations (c.G>A260 (p.Ser87Asn, H3S87N) mutations of canonical paralog *histone H3* genes) in clonally evolved B cells, we established knock-in mice (H3S87N KI) in which the Hist1h3c S87N mutant was inserted on the 3' UTR of the *Ighg1* promoter (supplemental Figure 9A–B). We confirmed the expression of H3S87N KI (supplemental Figure 9C). We observed H3S87N KI and wild-type mice under stimulation with sheep red blood cells every 4 weeks. Interestingly, at 15 weeks, the spleen of H3S87N KI was heavier than that of the wild type, accompanied by expanded follicular structures (supplemental Figure 9D–F). Furthermore, the percentages and number of GCB cells were significantly increased in the spleen of H3S87N KI compared to those of the wild type, whereas those of follicular B cells to marginal zone B cells were significantly increased in the spleen of H3S87N KI (supplemental Figure 9G). Cd40 expression on GCB cells collected from the spleen of H3S87N KI was higher than that in control mice (supplemental Figure 9H). These results suggest that core histone mutations acquired during clonal evolution contribute to expansion of GCB cells.

Supplemental Note2

Related to "Identification of the Cd40–Cd40lg interaction between GCB and T_{FH}-tumor cell clusters as a therapeutic target in T_{FH}-like lymphomas"

To explore the biological roles of CD40LG signaling in T cells, we performed whole-transcriptome analysis (WTA) using RNA extracted from Jurkat cells expressing the G17V mutant or mock ($Jurkat^{G17VRHOA}$ and $Jurkat^{mock}$) respectively[1], with or without stimulation by CD40-Fc chimera protein under stimulation by an anti-CD3 antibody: (1) $Jurkat^{mock}$ stimulated by anti-Cd3 antibody (Mock_CD3, n = 4), (2) $Jurkat^{mock}$ stimulated by anti-CD3 antibody and CD40-FC chimera (Mock_$CD3^{+}CD40^{FC}$, n = 4), (3) $Jurkat^{G17VRHOA}$ stimulated by anti-CD3 antibody (G17V_$CD3^{+}$, n = 4), and (4) $Jurkat^{G17VRHOA}$ stimulated by anti-CD3 antibody and Cd40-FC chimera (G17V _$CD3^{+}CD40^{FC}$, n = 4, supplemental Figure 11A). Principal component analysis revealed a distinct gene-expression pattern in each group (supplemental Figure 11B). We identified 341 differentially expressed genes (DEGs) between the G17V_$CD3^{+}CD40^{FC}$ and G17VRHOA_$CD3^{+}$ groups (up, n = 124; down, n = 217; supplemental Figure 11C–D), including oncogenic genes, such as *CDK6, TCF7*, and *VEGFA*. GSEA for WTA data showed that among hallmark and C6 oncogenic gene sets from MsigDB, 3 and 17 pathways were significantly enriched in the G17V_$CD3^{+}CD40^{FC}$ group compared with the G17VRHOA_$CD3^{+}$ group,

respectively. Among them, gene sets involved in mTOR, IL2 STAT5, and interferon gamma response signaling were enriched in the G17V_CD3^{+}CD40^{FC} group (supplemental Figure 11E–H). Furthermore, ingenuity pathway analysis (IPA) confirmed the enrichment of mTOR and VEGF signaling in the G17V_CD3^{+}CD40^{FC} group (supplemental Figure 11I).

Furthermore, to explore the effect of G17V *RHOA* mutation on CD40LG signaling in T cells, the G17V_CD3^{+}CD40^{FC} group was compared with Mock_CD3^{+}CD40^{FC}. GSEA for RNA-seq showed that 16 pathways were enriched in G17V_CD3^{+}CD40^{FC} compared with Mock_CD3^{+}. Notably, five pathways, including TNFA SIGNALING VIA NFKB and HEDGEHOG SIGNALING, were enriched only in G17V_CD3^{+}CD40^{FC} vs Mock_CD3^{+}CD40^{FC}, while enrichment of the other 11 pathways was also observed in G17V_CD3^{+} vs Mock_CD3^{+} (supplemental Figure 11J). Overall, these results suggest that CD40LG signaling in T cells stimulated by CD40 activates oncogenic pathways, such as the mTOR pathway, and contributes to tumorigenesis.

Supplemental Methods

Mouse genotyping

Genotyping and evaluation were performed using genomic DNA extracted from either tails (genotyping) using genomic PCR with the primers listed in supplemental Table 9.[2,3] This research was approved by the facility review committee (Approval number, 21-005). All strains were bred and housed under specific pathogen-free conditions. All animal experiments were performed according to the guidelines.

Human samples

Homeostatic lymph node (HLN) samples were prospectively collected from patients with solid tumors (n = 3) who had undergone lymph node (LN) resection between January and June 2020. LNs with no enlargement (< 1 cm) were used in this study. The collected LNs were confirmed to be negative for pan-cytokeratin using flow cytometry. Angioimmunoblastic T-cell lymphoma (AITL) samples (n = 6) were prospectively collected between March 2019 and July 2020. Lymphoma specimens were diagnosed by hematopathologists. Clinical characteristics of patients with HLN and AITL are listed in supplemental Table 10. This study was conducted in accordance with the Declaration of Helsinki and was approved by the review board of each

institution (Approval numbers, H24-075 and R01-209). Written informed consent was obtained from all participating patients.

Flow cytometric analysis

Mouse spleen tissue and LNs or human AITL LNs were manually minced and passed through a 70 μm cell strainer (Falcon) to prepare single-cell suspensions. The suspensions were dissolved in ammonium-potassium chloride buffer to remove red blood cells (RBCs). Multicolor flow cytometric analyses and sorting were performed on a BD FACS Aria II or Aria III sorter (BD Biosciences). FlowJo software (Tree Star Inc.) was used for all flow cytometric analyses.

Cell sorting

$Cd19^+B220^+Fas^+Gl\text{-}7^+Cd138^-$ GCB cells, $Cd19^+B220^+Fas^-Gl\text{-}7^-Cd138^-$ B cells excluding GCB cells (non-GCB cells), and $Cd4^+Cd8^-Pdcd1^+Icos^+$ T_{FH} cells were sorted from the spleen of MxTR. The purity of these preparations was > 95%. All antibodies used are listed in supplemental Table 11.

Transplantation of cell fractions isolated from the spleen of tumor-bearing MxTR

85 $Cd4^+$ cells, $B220^+$ cells, and $Cd11b^+$ cells were isolated from the spleens of tumor-bearing
86 MxTR using MACS beads (Cd4 [L3T4] MicroBeads, cat # 130-117-043; CD45R [B220]
87 MicroBeads, cat # 1130-049-501; and Cd11b MicroBeads, cat # 130-049-601; Miltenyi Biotec),
88 according to the manufacturer's instructions. After elution in MACS buffer, each single-cell
89 suspension was resuspended in RPMI-1640 Medium (RPMI, Sigma-Aldrich; concentration, $1 \times$
90 10^7 cells /mL). The cells in each fraction were mixed in 2×10^6 cells (200 μL). Ultimately, four
91 suspensions were prepared; **(i)** $Cd4^+$ (T), $B220^+$ (B), and $Cd11b^+$ cells (M); (ii) T and B; (iii) T
92 and M; (iv) T. In addition, no injection (v) and single-cell suspensions (2×10^7 cells) from the
93 spleen or LN of MxTR (vi) were prepared as positive and negative controls, respectively. Each
94 suspension was injected intraperitoneally into 5-week-old male nude mice (Charles River
95 Laboratory) irradiated with 2 Gy before infusion (supplemental Figure 2A). The nude mice used
96 in the experiment were housed under specific pathogen-free conditions. The donor H2kb (MHC
97 class I alloantigen from C57BL/6 mice) and the recipient H2kd (MHC class I alloantigen from
98 nude mice) in mononuclear cells of peripheral blood (PB) were used to identify the chimeras.
99 Chimerism of PB was checked on day 28 after transplantation. Successful engraftment was
100 defined as macroscopic splenomegaly and LN enlargement, and ≥ 1% of donor-derived
101 $Cd4^+H2kb^+$ cells in the mononuclear cells of PB.
102

Transplantation of GCB and T_{FH} cells isolated from tumor-bearing MxTR

GCB, non-GCB, and T_{FH} cells were sorted from the spleens of tumor-bearing MxTR. each single-cell suspension was resuspended in RPMI. The cells in each fraction were mixed in 2×10^5 cells (200 μL). Three types of mixed cells, i.e., (i) T_{FH} and GCB cells, (ii) T_{FH} and non-GCB cells, (iii) T_{FH} cells only, were injected intraperitoneally into 5-week-old male nude mice, which were treated with anti-asialo GM antibody (FUJIFILM) intraperitoneally, immediately prior to cell injection.[4] Nude mice were irradiated with 4 Gy, before injection. On day 7 after injection, chimerism in the spleen was assessed under the same conditions as before.

Antibody treatment

Single-cell suspensions (2×10^7 cells) prepared from spleen tissues of tumor-bearing MxTR were injected intraperitoneally into 5-week-old nude mice, irradiated with 2 Gy. Anti-Cd40lg antibody or Armenian hamster IgG isotype control (both from Bio X cell; 250 μg/mL prepared in PBS) was injected intraperitoneally every other day starting on day 0.

Immunofluorescence of mouse samples

Spleen tissues obtained from MxTR and MxWT were embedded in OCT (Sakura Finetek Japan Co.), immediately frozen in hexane cooled with dry ice, and stored at −80 °C. The spleen and

LNs were sectioned at a thickness of 2 μm on a cryostat at −16 °C. Sections were dried for 1 h at 25 °C, fixed for 10 min in 4% paraformaldehyde, permeabilized for 10 min with 0.1% Triton X-100, and blocked with 10% goat serum (Sigma-Aldrich) prepared in PBS for 30 min. Sections were stained overnight at 4 °C with the primary antibodies. After three washes, sections were stained for 1 h at 25 °C with the following secondary antibodies: AF488-goat-anti-rabbit IgG (Thermo Fisher Scientific) and AF594-goat-anti-rat IgG (Thermo Fisher Scientific). Potential tissue autofluorescence was quenched using the True VIEW Autofluorescence Quenching Kit (Vector Laboratories). After incubation with 4',6-diamidino-2-phenylindole (DAPI, Vectashield Mounting Medium; Vector Laboratories), the samples were imaged using a Leica TCS SP5 confocal laser scanning microscope (Leica Microsystems).

CD40LG stimulation

Jurkat cells inducibly expressing G17V RHOA mutant complementary DNA (cDNA) (Jurkat^{G17VRHOA}) and mock-transduced cells (Jurkat^{mock}) have been previously described[1]. Jurkat cells were cultured at 37 °C in RPMI supplemented with 10% fetal calf serum and 1% penicillin streptomycin. Twenty-four hours after induction with doxycycline 2 ug/mL, each indicated Jurkat line was rested for 4 hours in serum-free media. Cells were then collected and stimulated with recombinant human CD40/TNFRSF5-Fc chimeric protein

(R&D) or recombinant human IgG1 Fc protein (R&D) under the stimulation 2 ug/mL LEAF^{TM} purified anti-human CD3 antibody (BioLegend) for 24h at 37ºC. The collected cells were subjected to RNA-seq according to the protocols described.

Single-cell RNA sequencing (scRNA-seq) library preparation and sequencing for mouse samples

To examine immune cell profiles, Red-blood-cell (RBC)-free single-cell suspensions from the spleen of tumor-bearing MxTR (n = 2, MxTR1 and MxTR2) or MxWT (n = 2, MxWT1 and MxWT2) were converted into barcoded scRNA-seq libraries using Chromium Single Cell 3′ Reagent kits (10x Genomics, version 3.1), according to the manufacturer's instructions (CG000183 Rev A), aiming for ~5,000 cells per library. All libraries were subjected to quality control checks and quantified using the 2100 Bioanalyzer High Sensitivity DNA Kit (Agilent Technologies). The library information for each sample is listed in supplemental Table 12. Libraies were sequenced on the Illumina HiseqX platform.

scRNA-seq initial analysis

Regarding scRNA-seq data analysis, *Cell Ranger* pipelines (10x Genomics, version 3.1.0) were used to demultiplex raw data and to generate a matrix file of the features using barcodes. Matrix

157 data were analyzed with R using the R package *Seurat* v 3.1.0[5] on R Studio. Standard quality
158 control check was performed to remove cells with few genes or overexpression of mitochondrial
159 gene reads. Data normalization was performed using the "NormalizeData" function, and highly
160 variable features were extracted using the "FindVariableFeatures" function. Normalized data
161 were subjected to linear transformation (scaling) and principal component analysis (PCA),
162 based on variable features using the "ScaleData" and the "RunPCA" function. Graph-based
163 clustering of gene expression profiles was performed using the "FindNeighbors" and
164 "FindClusters" functions with default parameters. Nonlinear dimensionality reduction UMAP
165 with "RunUMAP" and "DimPlot" functions were used for visualization. In addition, the cell
166 clusters were annotated based on the expression of canonical markers, such as *Gzma*, *Cxcr3*,
167 and *Dapl1* for Cd8 T cells; *Ccl3*, *Cd28*, and *Pdcd1* for Cd4 T cells; *Ighd*, *Icosl*, *Cr2*, *Parm1*,
168 *Cd83*, and *Prdm1* for B cells; and *Adgre1*, *Ifitm3*, and *S100a9* for myeloid cells.
169
170 **Data integration for scRNA-seq and batch correction**
171 Canonical correlation analysis (CCA) was performed to identify shared sources of variation
172 across multiple datasets using the "FindIntegrationAnchors" function.[5] Four datasets (data from
173 spleen cells of MxTR [n = 2] and MxWT [n = 2] mice) were integrated using the anchors by the

174 “IntegrateData” function with canonical correlation dimensions of 20. Integrated data were
175 scaled and subjected to PCA as described above.
176
177 **scRNA-seq of human samples**
178 Two of the 5 AITL samples (AITL1 and AITL2) and the 3 HLN samples (HLN1, HLN2, and
179 HLN3) were converted into barcoded scRNA-seq libraries using Chromium Single Cell 3’
180 Reagent kits, and 3 of the 5 AITL samples (AITL3, AITL4, and AITL5) were converted using
181 Chromium Single Cell 5’ Reagent kits (10x Genomics, version 1.1). *Cell Ranger* pipelines were
182 used to demultiplex raw data and to generate a matrix file of the features using barcodes. Eight
183 datasets (data from AITL [n = 5] and HLN [n = 3]) were integrated using anchors by the
184 “IntegrateData” function with canonical correlation dimensions of 20. Quality control and PCA
185 were performed using the same strategy employed for the scRNA-seq analysis of mice.
186
187 **Gene set variation analysis (GSVA) of scRNA-seq data**
188 Significantly enriched pathways for scRNA-seq data were analyzed using the *GSVA* ver. 1.38.0.[6]
189 The average gene expression data of each cluster were analyzed, and the activity scores for each
190 cluster were compared using a generalized linear model (GLM). GLM output was visualized via
191 heatmaps, which were constructed using the R package *heatmap3*[7].

Differentially expressed gene (DEG) analysis of scRNA-seq

DEG analysis between MxTR vs MxWT or AITL vs HLN was performed in each cluster using "FindMarkers" or "FindAllMarkers" functions as appropriate, with a minimum percentage of gene-expressing cells set to 20%; the minimum log fold-change in gene expression in each cluster, in comparison to that in all the other clusters was set to 0.25. DEGs were defined as genes with an adjusted p-value < 0.05. The results of the Wilcoxon rank-sum test were used to construct the DEG lists and volcano plots. Volcano plots were plotted using the R package *ggplot2*.

To identify pathways significantly enriched in each group, *Gene Set Enrichment Analysis* (*GSEA* 4.1.0, https://www.gsea-msigdb.org/gsea/index.jsp) and *Metascape* (https://metascape.org/gp/index.html#/main/step1) were used.

Cell–cell interaction analysis of scRNA-seq data

We analyzed cell–cell interactions between immune cell clusters and T_{FH}-tumor cell cluster using the *CellPhoneDB* package,[8] a manually curated repository of ligands, receptors, and their interactions, integrated with a statistical framework for inferring intercellular interactions from single-cell transcriptomes.[9] Briefly, potential ligand–receptor interactions were statistically

selected based on the expression of a receptor gene in a lineage subpopulation and a ligand gene in another. We only considered genes expressed in > 20% of cells in any given subpopulation. We permuted the cluster labels of all input cells 1,000 times and calculated the mean interaction score (the average receptor expression level in a subpopulation multiplied by the average ligand expression level in the interacting subpopulation), generating a null distribution of the mean interaction score for each ligand–receptor pair in each pairwise comparison across subpopulations. We located observed mean interaction scores that were the same or higher than the actual mean score in the null distribution. We calculated the proportion of the observed scores, conferring a *p*-value for the likelihood of specificity of a given ligand–receptor complex to a given cluster pair.

RNA sequencing (RNA-seq)

GCB cells were isolated from the spleens of tumor-bearing MxTR (n = 4) or MxWT (n = 3) mice. Total RNA was extracted using the RNeasy Mini Kit (Qiagen). RNA integrity number (RIN) values were analyzed using the Agilent 2100 Bioanalyzer (Agilent Technologies); samples with an RIN > 8 were used in subsequent analyses. Libraries were prepared using a SMARTer Stranded Total RNA-seq Kit v2—Pico Input Mammalian (Takara Bio Inc.) or a TruSeq RNA Sample Preparation Kit (illumina) according to the manufacturer's instructions.

The concentration and size distribution of the libraries were assessed using an Agilent 2100 Bioanalyzer (Agilent Technologies). Sequencing was performed using the Illumina HiSeq X platform with a standard 150 bp paired-end read protocol at Macrogen or Illumina NextSeq 500 platform with a paired-end 36-base read option at Tsukuba i-Laboratory LLP (Ibaraki, Japan), and then analyzed using the CLC workbench version 9.5.1 (Qiagen). Sequencing reads were trimmed to remove adapter sequences from the 3′ ends of reads, mapped onto the reference genome (GRCm38), and quantified. For each gene, reads per kilobase of exon per million mapped reads (RPKMs) were normalized, estimated as exons per kilobase, and filtered using the Empirical Analysis of Digital Gene Expression tool. DEG analysis and GSEA were analyzed using the protocol written in scRNAseq data analysis.

Raw data for RNA-seq data from GCB cells of Vav-Cre/Tet2$^{-/-}$ or Vav-Cre/Tet2$^{+/+}$, and human diffuse large B-cell lymphoma (DLBCL) samples were downloaded from Gene Expression Omnibus (GSE111700)[10] and European Genome-Phenome Archive (EGAS00001002606)[11] and reanalyzed, respectively.

Whole exome sequencing (WES)

Genomic DNA was extracted using the QIAamp DNA Blood Mini Kit (Qiagen) from 1×10^5 GCB and T_{FH} cells from the spleen of tumor-bearing MxTR (n = 6) or paired tail tissue as the

246 reference. Genomic DNA was extracted from the LNs of AITL patients (n = 5) and sorted four
247 B-cell fractions (n = 2), including naïve B ($IgD^+CD19^+CD138^-$), memory B ($IgD^-CD38^-CD10^-$
248 $CD19^+CD138^-$), GCB ($IgD^-CD38^-CD10^+CD19^+CD138^-$), and plasma cell fractions
249 ($CD19^{dull}CD138^+$) using a QIAamp DNA Blood Mini Kit. DNA integrity number (DIN) values
250 were examined using Agilent TapeStation 2200 (Agilent Technologies); samples with a DIN
251 number > 8 were included for subsequent analyses. Libraries were prepared from 100 ng
252 genomic DNA sheared using a Covaris S220 sonicator (M&S Instruments Inc.). SureSelect XT
253 Mouse All Exon kits (Agilent Technologies) were used for exon capture, according to the
254 manufacturer's instructions for mouse DNA. Sequencing data were generated using a standard
255 150 bp paired-end protocol on the Illumina HiSeq X or NovaSeq 6000 platform. Sequence
256 alignment and mutation calling were performed using the *Genomon2* pipeline
257 (https://github.com/Genomon-Project). The sequencing reads were mapped onto the reference
258 genome (GRCm38). Putative somatic mutations with an EB call *p*-value > 2.0, and Fisher's
259 exact *p*-value < 0.01 were considered. Mapping errors were excluded by visual inspection using
260 *Integrative Genomics Viewer* (*IGV*, version 2.6.2).[12]
261 Four genomic DNA samples from AITL were subjected to WES, using a protocol
262 similar to that used for analyzing mice samples, using SureSelect XT Human All Exon kits
263 (Agilent Technologies). GRCh38 was used as the reference genome.

Immuno-profiling analysis using bulk RNA-seq and WES data

The *MiXCR* algorithm[13] was used for immune profiling of bulk RNA-seq data of mouse GCB cells and WES data of mouse T_{FH} and GCB cells. Then, we extracted hypervariable complementarity-determining region 3 (CDR3) sequences and the VDJ gene segment of the *T-cell receptor (TCR)* and *immunoglobulin (Ig)* genes. *TCR* and *Ig* sequences identified using *MiXCR* were analyzed using the R package, *LymphoSeq,*[14] and visualized.

Whole-genome bisulfite sequencing (WGBS)

GCB cells sorted from the spleens of tumor-bearing MxTR (n = 2) and MxWT (n = 2) mice were used for library preparation. Library preparation for WGBS was performed using the post-bisulfite adaptor tagging (PBAT) strategy.[15] Genomic DNA was extracted from 5,000 sorted cells using a QIAamp DNA Blood Mini Kit (Qiagen). The number of cells was limited; and therefore, the library was prepared without quantifying the DNA yield. Four-fifths of the volume of purified genomic DNA was spiked with 300 pg unmethylated lambda DNA (Promega) and used for bisulfite treatment using the EZ DNA methylation gold kit (Zymo Research). The tPBAT protocol was performed as described previously.[16] After library preparation, library yields were determined using the library quantification kit (Takara Bio Inc.).

Four cycles of PCR amplification were performed using PrimeStar Max DNA polymerase (Takara Bio Inc.), and the amplified libraries were sequenced on the Illumina HiSeq X platform at Macrogen. One quarter of the sequencing lanes were assigned per sample. Sequenced reads were analyzed as described previously.[15] The basic metrics of the methylome data are provided in supplemental Table 13.

Data Availability

Sequencing files are deposited in the European Nucleotide Archive ERP138895 or the European Genome-phenome Archive EGAS00001006401.

Code Availability

Scripts used for data analysis are available upon request.

Supplemental Table Legends

Supplemental Table 1. Top 50 markers highly expressed in each cluster

Supplemental Table 2. Hyper-DMRs in GCB cells from MxTR compared to those from MxWT

Supplemental Table 3. Hypo-DMRs in GCB cells from MxTR compared to those from MxWT

Supplemental Table 4. Clonotyping based on CDR3 sequences performed for Igh genes in RNA-seq data of MxTR1 and MxWT1

Supplemental Table 5. Somatic mutations detected by WES for T_{FH} and GCB cells sorted from tumors of five MxTR

Supplemental Table 6. Somatic mutations detected by WES for the LNs of AITL patients and sorted four B-cell fractions

Supplemental Table 7. Differential expression genes from hB1–9 of scRNA-seq

Supplemental Table 8. Gene sets that characterize B cells, especially GCB cells

(A) GCB-related gene sets cited from Holmes et al.

(B) AITL-B-specific gene set

(C) T cell signature gene sets from Chung et al.

(D) T_{FH}-tumor cell signatures from Nguyen et al.

(E) B cell signature gene sets from Chung et al.

Supplemental Table 9. Sequences of primers used in the study

Supplemental Table 10. Demographics and clinical and phenotypic characteristics of HLN and AITL cohort

Supplemental Table 11. Antibodies used for flow cytometric analysis and immunofluorescence staining

Supplemental Table 12. Sequencing metrics for the study cohort as determined by *Cell Ranger*

Supplemental Table 13. Basic statistics of methylome data

Supplemental Figure 1

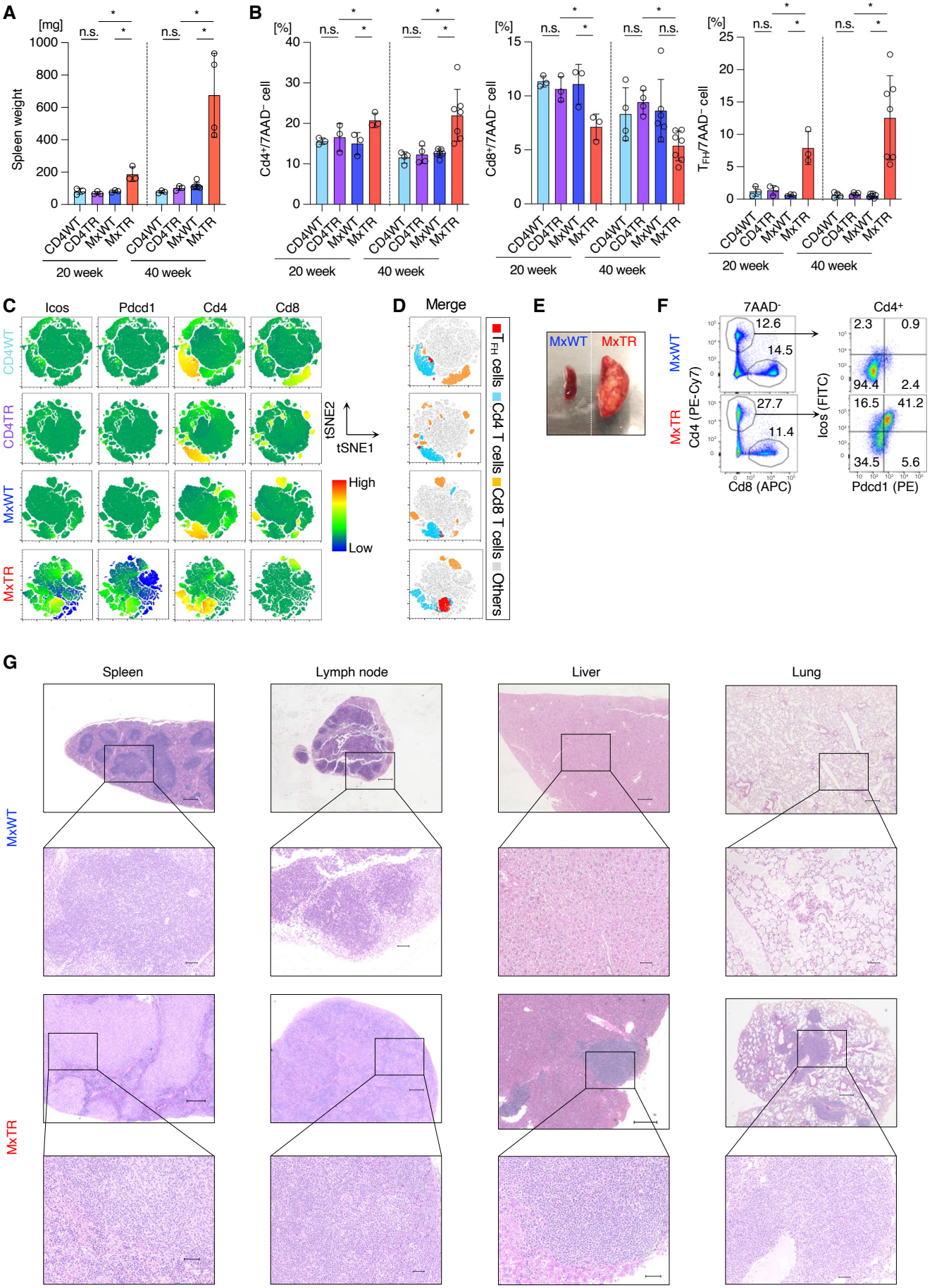

Supplemental Figure 1. Contribution of *Tet2*-deficient immune cells in the development of T_{FH}-like lymphomas

(A) Spleen weights of mice at 20 and 40 weeks of age.

(B) The proportions of $Cd4^+$, $Cd8^+$, and $Cd4^+Cd8^-Pdcd1^+Icos^+$ (T_{FH}) cells determined using flow cytometry at 20 and 40 weeks of age.

(C) Representative tSNE heatmaps of the flow cytometric data of T-cell fractions in the spleen at 40 weeks of age. The expression of cell surface markers, including Icos, Pdcd1, Cd4, and Cd8.

(D) tSNE plots of manually gated and integrated T_{FH} (red), $Cd4^+$ (light blue), $Cd8^+$ (orange) cells, and others (grey) using data from supplemental Figure 1C.

(E) Macroscopic analysis of representative spleens from tumor-bearing MxTR and MxWT at 50 weeks of age.

(F) Representative flow cytometric plots of Cd4, Cd8, Icos, and Pdcd1 in spleen cells from tumor-bearing MxTR and MxWT at 50 weeks of age.

(G) Low (×4, top) and high (×20, bottom) magnification images showing hematoxylin and eosin (HE) staining of spleen, lymph node, liver, and lung tissue from tumor-bearing MxTR and MxWT at 50 weeks of age. Scale bar; 300 μm (top), 50 μm (bottom).

Supplemental Figure 2

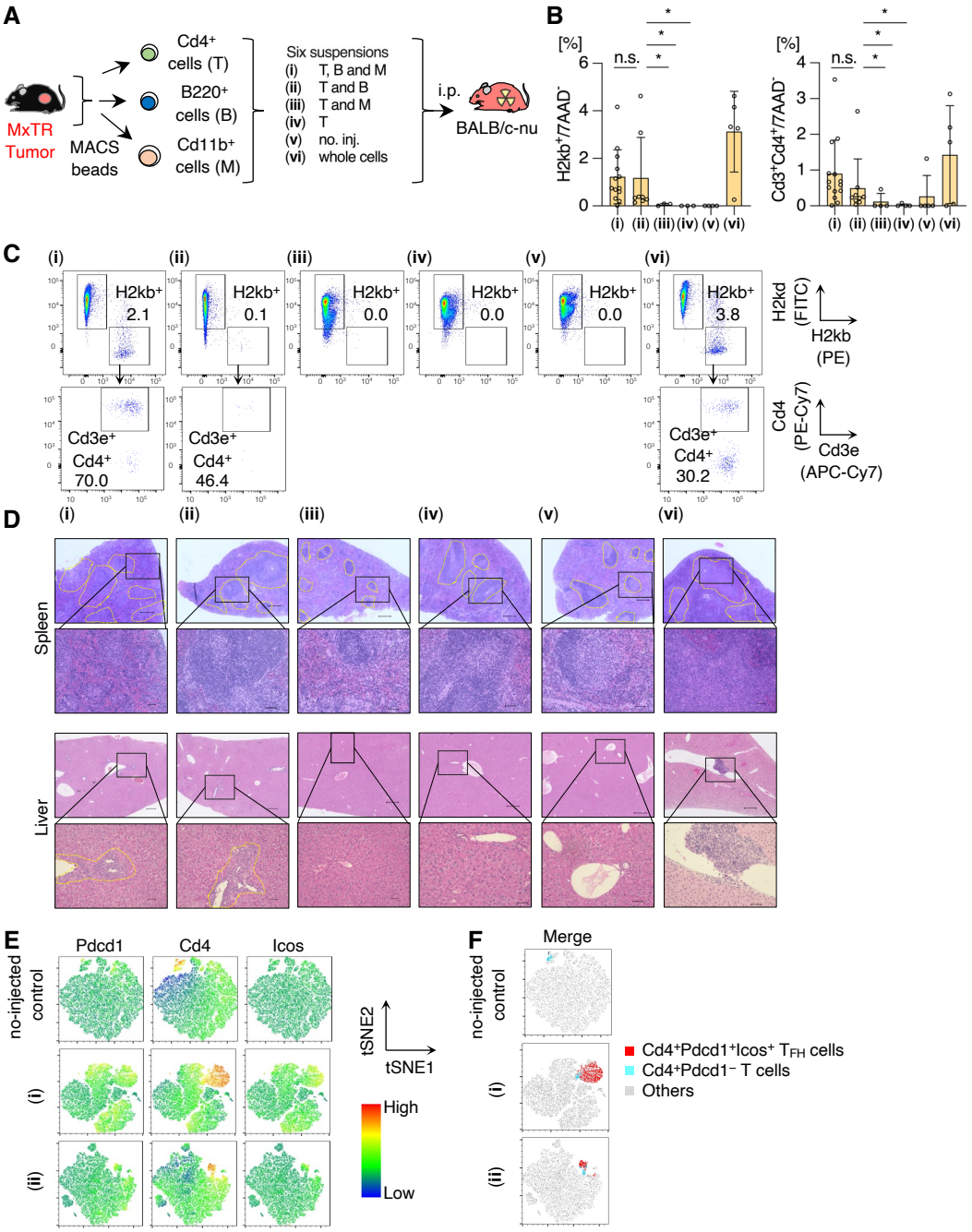

Supplemental Figure 2. Transplantation with fractionated cells sorted from tumors of MxTR

(A) Overview of workflow for transplantation of nude mice with $Cd4^+$, $B220^+$, and $Cd11b^+$ cells sorted from tumors of MxTR. i.p., intraperitoneal injection.

(B) Proportions of donor-derived $H2kb^+$ and $H2kb^+Cd3^+Cd4^+$ cells 4 weeks after injection. Six groups (i–vi) represent (i) $Cd4^+$ cells [T], $B220^+$ cells [B], and $Cd11b^+$ cells [M]; (ii) T and B; (iii) T and M; (iv) T; (v) no injection; and (vi) whole cells (positive controls).

(C) Representative flow cytometric plots of $H2kd^+$ recipient-derived markers, $H2kb^+$ donor-derived markers, and $H2kb^+Cd3e^+Cd4^+$ cells in i to vi (Six groups (i–vi) are the same as in supplemental Figure 2B.).

(D) Low (×4, top) and high (×20,bottom) magnification images showing hematoxylin and eosin (HE) staining of spleen and liver tissue from i to vi (Six groups (i–vi) are the same as in supplemental Figure 2B.). Splenic follicles and liver infiltration are indicated by yellow dotted lines. Scale bar; 300 μm (top), 50 μm (bottom).

(E) Representative tSNE heatmaps of flow cytometric data from spleen cells from uninjected control, (i), and (ii) at 4 weeks after transplantation. The expression of cell surface markers, including Icos, Pdcd1, and Cd4 (Two groups (i and ii) are the same as in supplemental Figure 2B.).

(F) tSNE plots of manually gated and integrated T_{FH} (red), $Cd4^{+}Pdcd1^{-}$ T cells (light blue), and others (grey) using data from supplemental Figure 2E.

For all panels, * *p*-value < 0.05; n.s. not significant.

Supplemental Figure 3

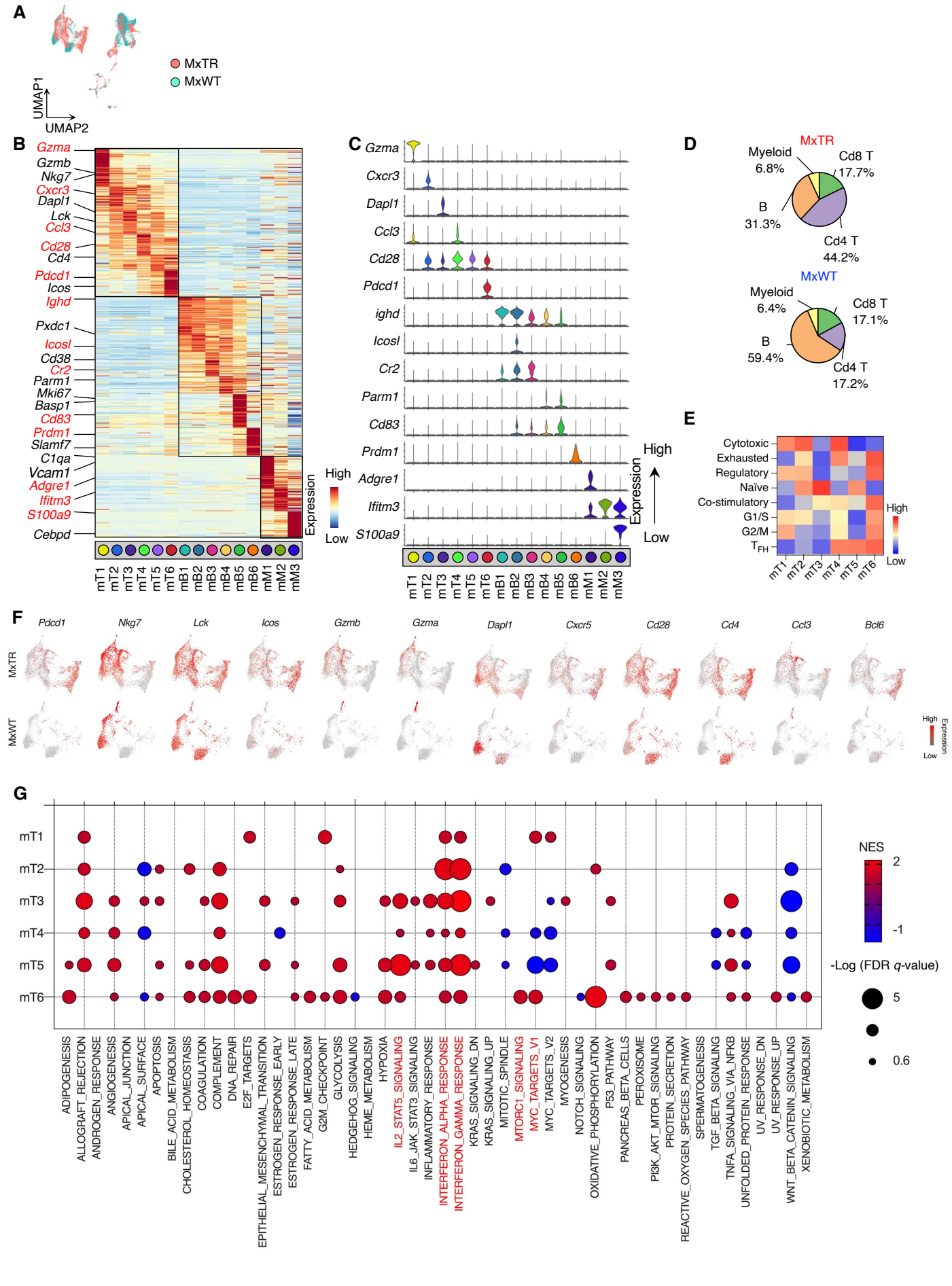

Supplemental Figure 3. Analysis of intratumor heterogeneity in spleen cells from tumor-bearing MxTR or MxWT using single-cell RNA sequencing (scRNA-seq)

(A) UMAP plot showing integrated scRNA-seq data from spleen cells from tumor-bearing MxTR and MxWT.

(B) Heatmap of top 50 conserved markers in each cluster. Rectangle group clusters from each cell type. Genes in red represent specific conserved markers in each cluster. Top 50 markers highly expressed in each cluster are listed in supplemental Table 1.

(C) Stacked violin plots showing specific conserved markers in each cluster.

(D) Pie charts showing the proportions of Cd8 T, Cd4 T, B, and myeloid cells in the MxTR and MxWT samples.

(E) GSVA with T-cell related gene sets from Chung et al. and T_{FH}-tumor cell signatures from Neguyen at al. Gene sets are listed in supplemental Table 8.

(F) Feature plots for markers characteristic of T cells.

(G) Dot plots showing pathways upregulated in mT1–6 from MxTR compared to that from MxWT, using GSEA with hallmark gene sets of MsigDB. Dot size indicates -Log(FDR *q*-value).

Supplemental Figure 4

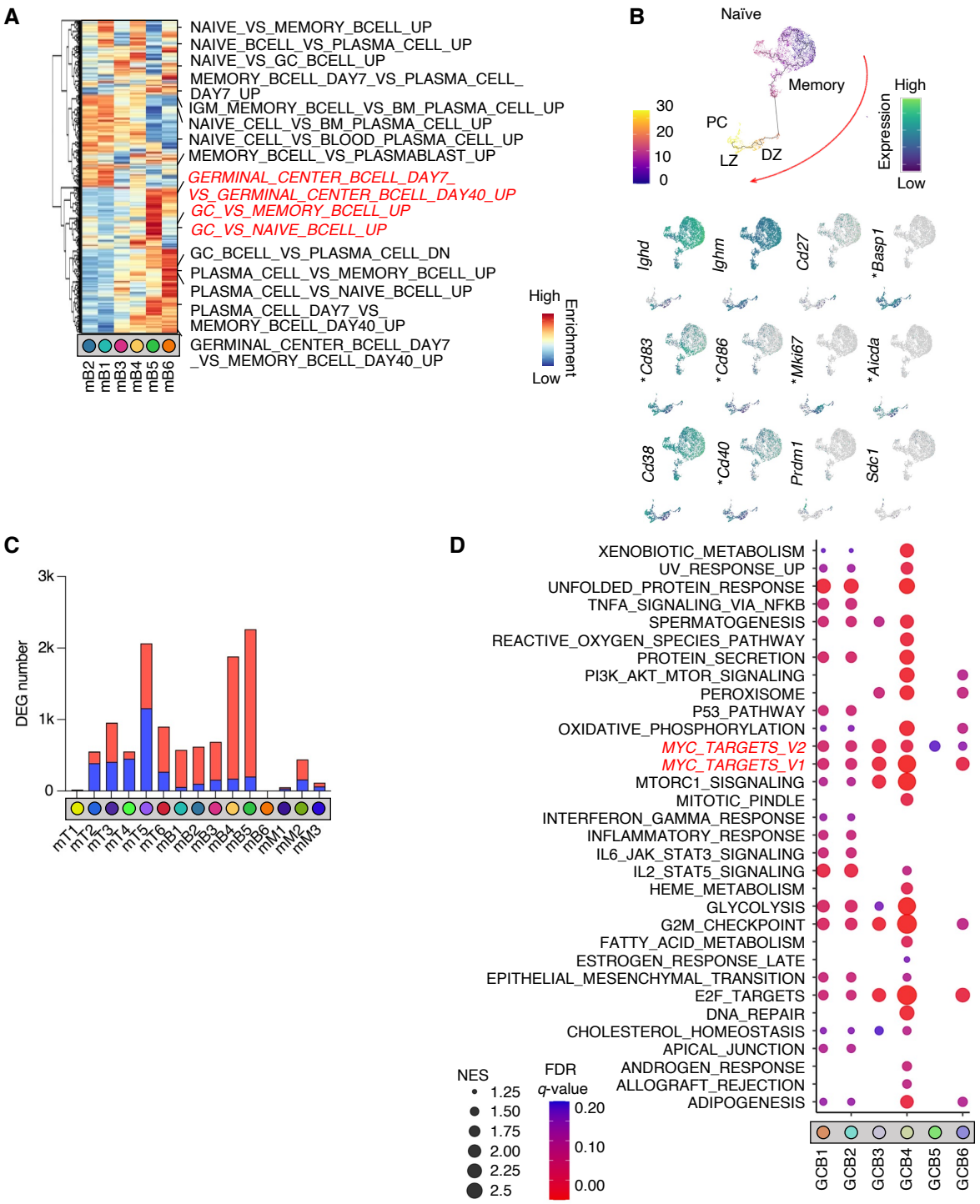

Supplemental Figure 4. Transcriptomic heterogeneity in B-cell subclusters of T_{FH}-like lymphomas

(A) Heatmap showing pathways differentially enriched in each B-cell cluster (mB1–6) by GSVA with C7 gene sets of MsigDB. Gene sets in red indicate pathways enriched in mB5.

(B) scRNA-seq data focusing on B cells, indicating B-cell differentiation steps using pseudo-time analysis and representative feature plots. Dark winding lines in the UMAP plots indicate the presumed developmental trajectories. * GCB-related markers.

(C) Bar graphs showing the number of differentially expressed genes (DEGs) upregulated in MxTR (red) and MxWT (blue) samples.

(D) Dot plots showing pathways upregulated in GCB1–6 from MxTR compared to that from MxWT, using GSEA with hallmark gene sets of MsigDB. Dot size indicates NES. Cut-off, FDR q-value < 0.25.

Supplemental Figure 5

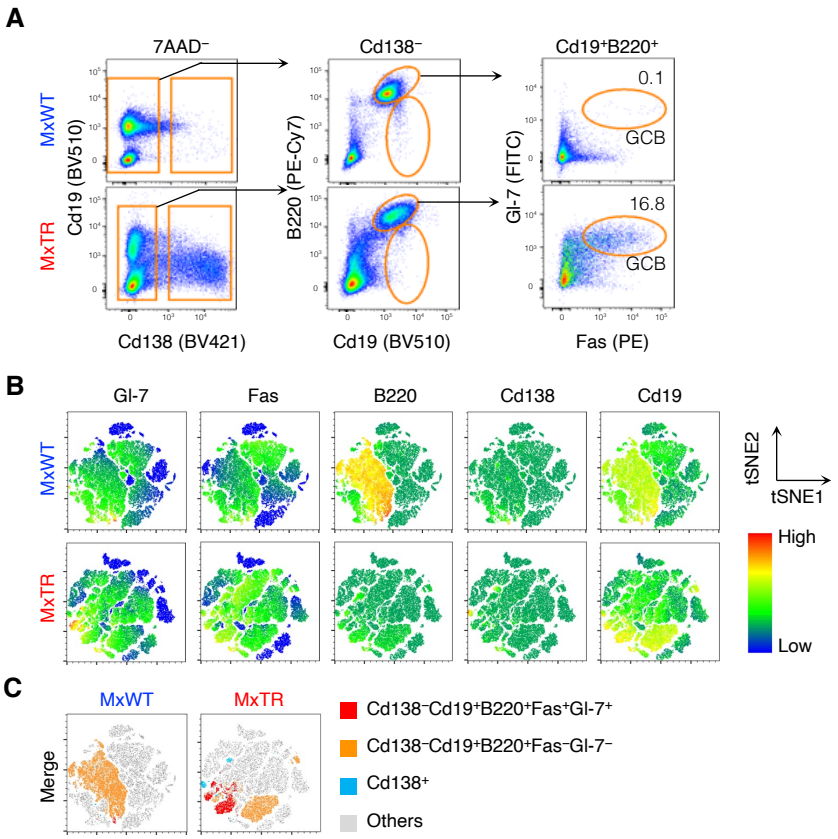

Supplemental Figure 5. Flow cytometric analysis of B-cell fractions in spleen cells from MxTR and MxWT

(A) Representative flow cytometry plots of Cd138, Cd19, B220, Fas, and Gl-7 in spleen cells from tumor-bearing MxTR and MxWT at ~50 weeks of age.

(B) Representative tSNE heatmaps of flow cytometric data of Cd138, Cd19, B220, Fas, and Gl-7 in spleen cells of tumor-bearing MxTR and MxWT at ~50 weeks of age.

(C) tSNE plots of manually gated and integrated $Cd138^{-}Cd19^{+}B220^{+}Fas^{+}Gl\text{-}7^{+}$ (red), $Cd138^{-}Cd19^{+}B220^{+}Fas^{-}Gl\text{-}7^{-}$ (orange), $Cd138^{+}$ (light blue) cells, and others (grey) using data from supplemental Figure 5B.

Supplemental Figure 6

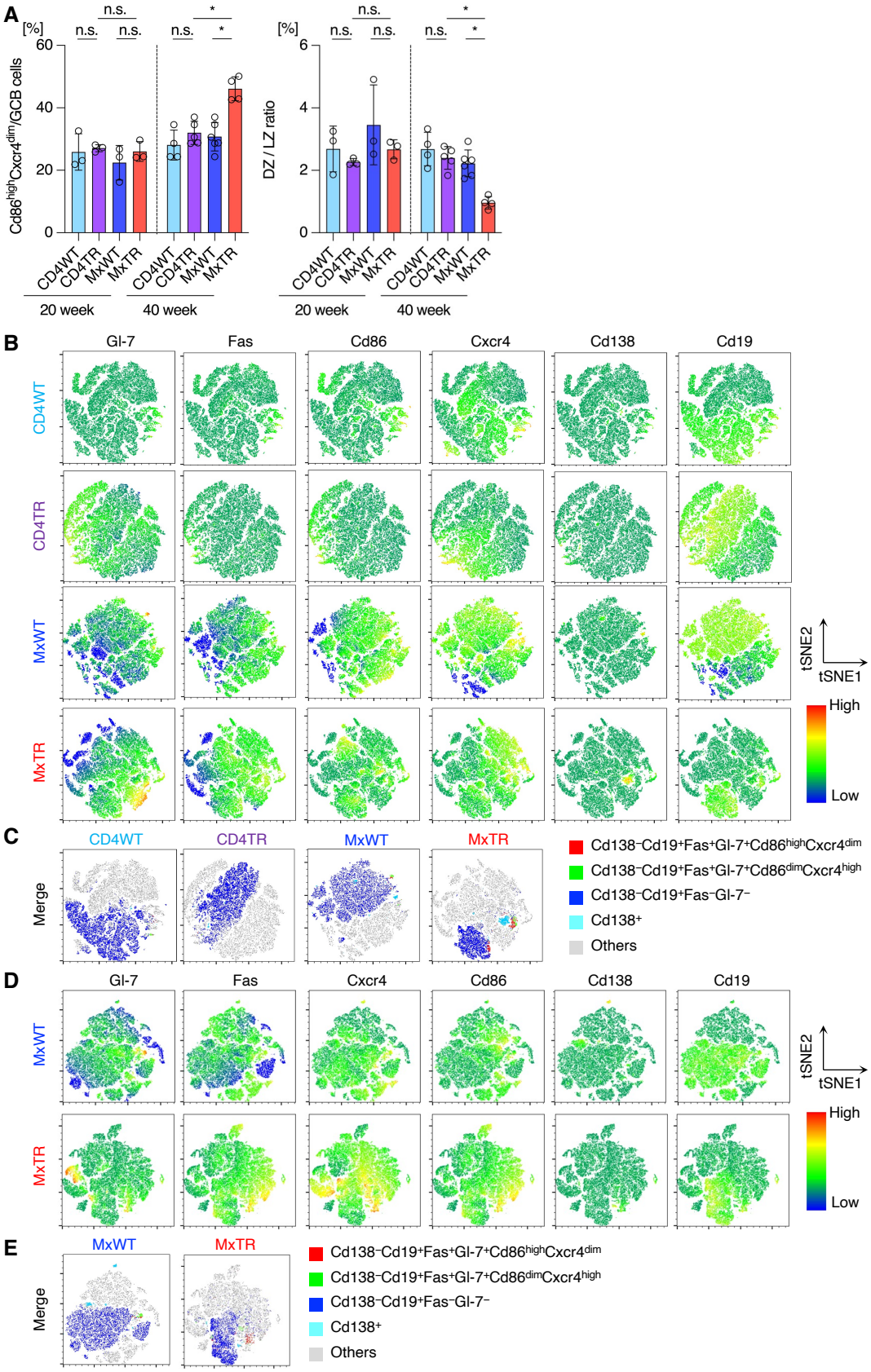

Supplemental Figure 6. Flow cytometric analysis of GCB fractions in spleen cells from MxTR and MxWT

(A) Proportions of $Cd86^{high}Cxcr4^{dim}$ light zone (LZ) /total GCB cells and $Cd86^{dim}Cxcr4^{high}$ dark zone (DZ)/LZ GCB cells in spleen cells from mice of the indicated genotypes at 20 and 40 weeks of age. MxTR, n = 6; MxWT, n = 4; CD4TR, n = 4; CD4WT, n = 5.

(B) Representative tSNE heatmaps of flow cytometric data of GCB fractions found in spleen cells from mice with the indicated genotypes at 40 weeks of age. The cell surface markers Gl-7, Fas, Cd86, Cxcr4, and Cd138, indicated GCB cells or plasma cells (PCs).

(C) tSNE plots of manually gated and integrated $Cd138^{-}Cd19^{+}Fas^{+}Gl\text{-}7^{+}Cd86^{high}Cxcr4^{dim}$ (red), $Cd138^{-}Cd19^{+}Fas^{+}Gl\text{-}7^{+}Cd86^{dim}Cxcr4^{high}$ (light green), $Cd138^{-}Cd19^{+}Fas^{-}Gl\text{-}7^{-}$ (blue), $Cd138^{+}$ (light blue) cells, and others (grey) using data from supplemental Figure 6B.

(D) Representative tSNE heatmaps of flow cytometric data of Cd138, Cd19, Fas, Gl-7, Cxcr4, and Cd86 in spleen cells from tumor-bearing MxTR and MxWT at ~50 weeks of age.

(E) tSNE plots of manually gated and integrated $Cd138^{-}Cd19^{+}Fas^{+}Gl\text{-}7^{+}Cd86^{high}Cxcr4^{dim}$ (red), $Cd138^{-}Cd19^{+}Fas^{+}Gl\text{-}7^{+}Cd86^{dim}Cxcr4^{high}$ (light green), $Cd138^{-}Cd19^{+}Fas^{-}Gl\text{-}7^{-}$ (blue), $Cd138^{+}$ (light blue) cells, and others (grey) using data from supplemental Figure 6D.

Supplemental Figure 7

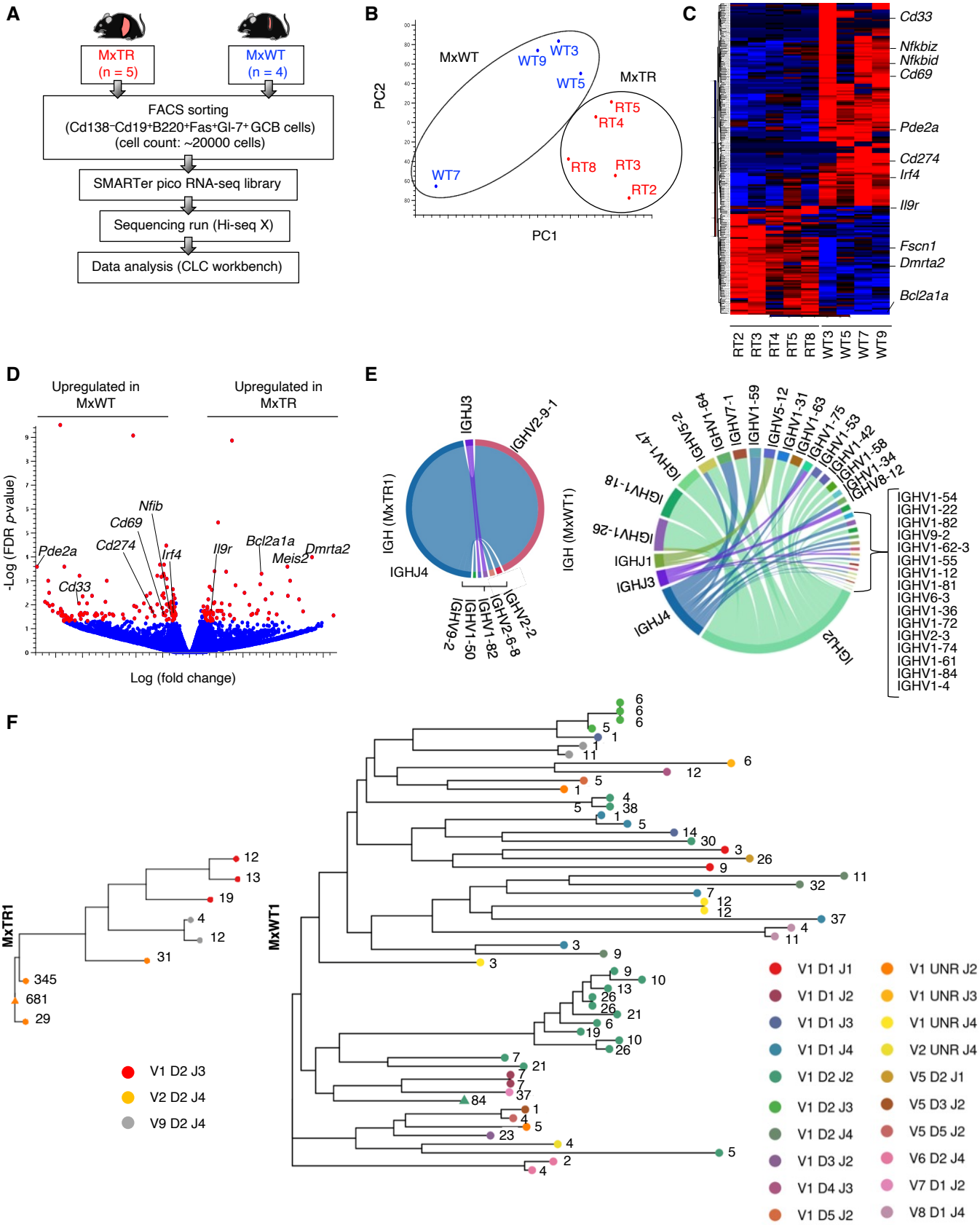

Supplemental Figure 7. RNA-seq analysis of GCB cells sorted from tumor-bearing MxTR and MxWT

(A) Overview of RNA-seq for GCB cells in spleen cells from MxTR (n = 5) and MxWT (n = 4) mice.

(B) PCA plot for RNA-seq. Blue dots, MxWT; red dots, MxTR.

(C) Unsupervised hierarchical clustering analyses of RNA-seq data for GCB cells from MxTR and MxWT.

(D) Volcano plot of up- or down-regulated genes in GCB cells from MxTR and MxWT. Cut-off; FDR *p*-value ≥ 0.1 with LogFC > |2| (red), FDR *p*-value < 0.1, or LogFC ≤ |2| (blue).

(E) Chord diagrams showing associations between *Ighv* and *Ighj* genes in GCB cells from MxTR1 and MxWT1 mice, respectively.

(F) Phylogenetic trees showing *Igh* expression in MxTR1 (left) or MxWT1 (right) GCB cells. Branches are color-coded to indicate V, D, and J gene usage. Numbers next to each branch refer to the sequence count.

Supplemental Figure 8

A

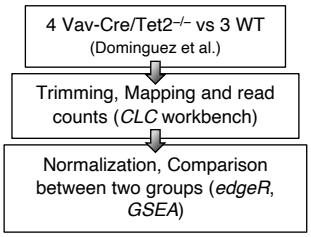

B

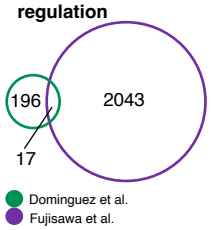

17 genes

Serpinb6b	*Atad5*
Ighg1	*Gadd45g*
Esco2	*Cadm1*
Gm47283	*Slco4a1*
Nfil3	*Rnf19b*
Cabin1	*Bcat1*
Mid1	*Gm14296*
Parp8	*Pidd1*
Dkk3	

28 genes

Lefty1	*Snn*	*Ly86*
Ogfrl1	*Gm2a*	*Klf3*
Rell1	*Fcmr*	*Ctsb*
Cd36	*Lmo2*	*Cnn3*
Cyba	*Ms4a4c*	*Atp1b1*
Akap12	*Cd55*	*Kctd12*
Cnr2	*Sell*	*Hhex*
4930523C07Rik	*Pdcd4*	*Ly6d*
S100a10	*Serpinb1a*	*Plac8*
Egr3		

C

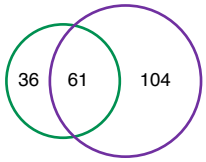

Shared gene sets (Top 10)

GC_T_HELPER_UP2X_CHTANOVA
C1.CREBBP.DOWN_397
GC_T_HELPER_UP4X_CHTANOVA
QUIESCENCE_HEME_CLUSTER1
MOUSE_SHCREBBP.R2.DOWN_545
NB_GCB_PROGRESSION_ALL_GENES_RPKM_MINUS5
NFKB_ALL_OCILY3_LY10
GCB_BCL6SMRT_DISTAL_ENHANCER
TCELL_CYTOKINE_INDUCED_IL2_IL7_IL15ONLY
BLOOD_CD4+TCELL_GT_THYMIC_SP_CD4+TCELL

D

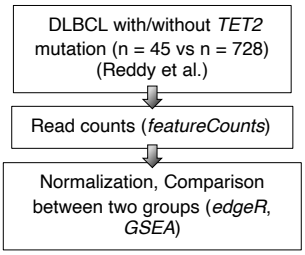

E

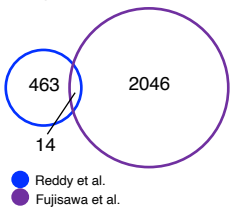

14 genes

PHYH/ Phyh	*DUSP10/ Dusp10*
FYTTD1/ Fyttd1	*MDH1/ Mdh1*
COMMD3/ Commd3	*SEC61B/ Sec61b*
SIAH2/ Siah2	*CADM1/ Cadm1*
OTULIN/ Otulin	*AKAP5/ Akap5*
SLC24A5/ Slc24a5	*TMED8/ Tmed8*
DNAJA2/ Dnaja2	*NUP133/ Nup133*

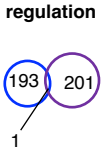

1 gene

PLAC8/ Plac8

F

Shared gene sets (Top 10)

PROLIFERATION_NODE1618
CELL_CYCLE_LIU
CELL_CYCLE_CHO&WHITFIELD
MYELOMA_PR_SUBGROUP_UP
MCL_PROLIFERATION_SURVIVAL
CELL_CYCLE_WHITFIELD
STAT3HIGH_ABC_DLBCL_SUBGROUP
LIVER_FETAL_LUNG_NODE1634
TCELL_CYTOKINE_INDUCED_PROLIF
MUSCLE_NODE1645

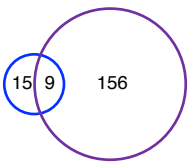

Shared gene sets

RESTING_PANT_CELL_CD4+CD8+_GNF
T_CELL
T_NK_NODE1604
TCELL_CYTOKINE_REPRESSED
GC_B_CELL_BLHIGH_DLBCLLOW
FOLLICULAR_LYMPHOMA_IMMUNE_RESPONSE1
ABC_GT_GCB_AFFY
GLUCOSE_STARVE_UP
KLF2_INDUCED

Supplemental Figure 8. Comparison between RNA-seq data of GCB cells from MxTR and those from Vav-Cre/Tet2$^{-/-}$ or human DLBCL with *TET2* mutation.

(A) Scheme for reanalysis of RNA-seq data for Vav-Cre/Tet2$^{-/-}$ and VAV1-Cre/Tet2$^{+/+}$ (WT).

(B) Venn diagram showing shared genes significantly up- or downregulated in Vav-Cre/Tet2$^{-/-}$ (green) and MxTR (purple) relative to each wild type, respectively. Shared genes are listed.

(C) Venn diagram showing shared gene sets significantly enriched in Vav-Cre/Tet2$^{-/-}$ (green) and MxTR (purple) relative to each wild type, respectively.[17]

(D) Scheme for reanalysis of RNA-seq data for human DLBCL samples with/without *TET2* mutations. Shared genes are listed.

(E) Venn diagram showing common genes significantly up- or downregulated in DLBCL with *TET2* mutations (blue) and GCB cells from and MxTR (purple).

(F) Venn diagram showing common gene sets significantly enriched in DLBCL with *TET2* mutations (blue) and GCB cells from and MxTR (purple). Shared gene sets are listed.

Supplemental Figure 9

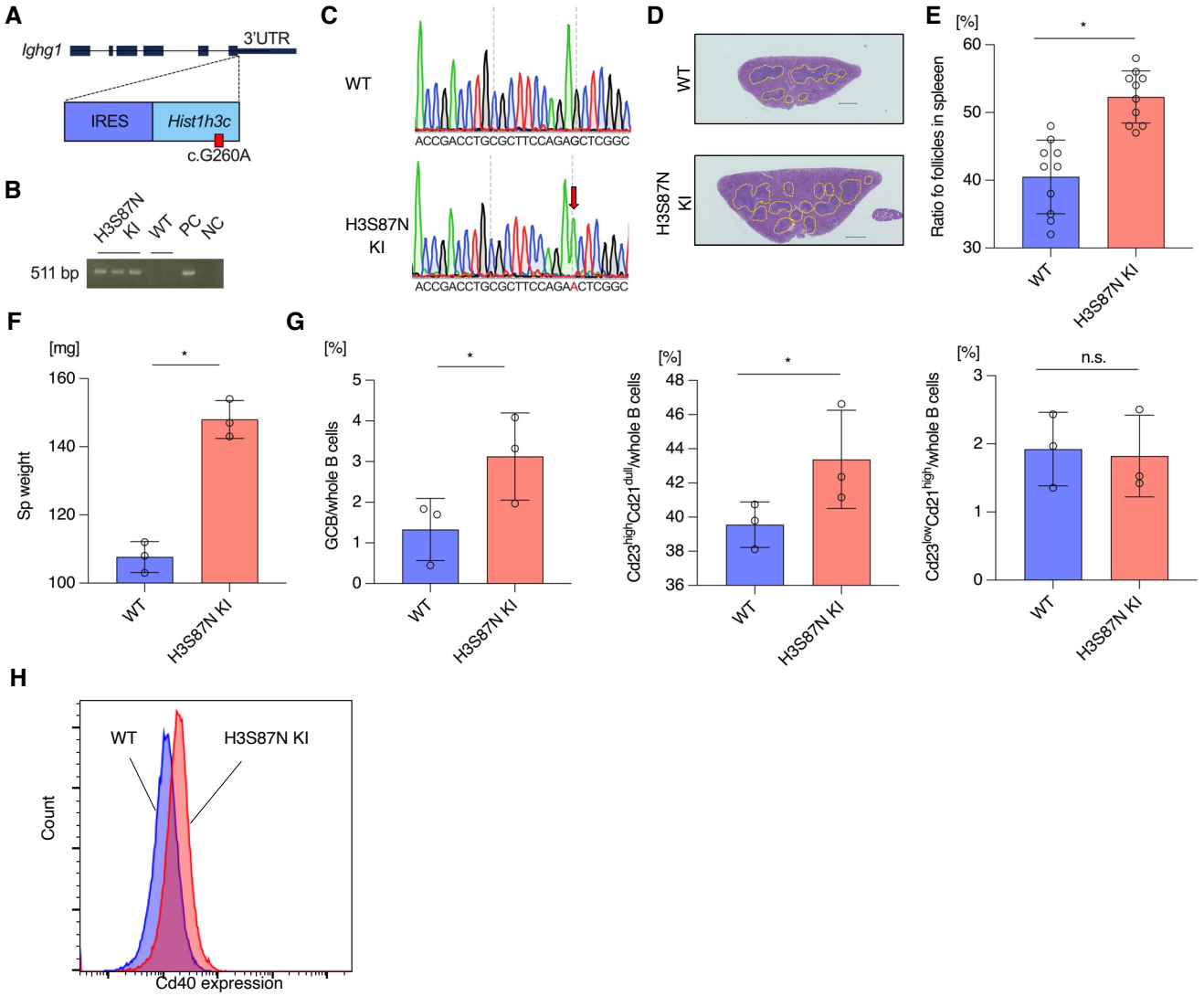

Supplemental Figure 9. Expansion of GCB cells in H3S87N KI

(A) A structure of the *Hist1h3c* S87N (c.G>A260) mutant vector inserted on the 3' UTR of the *Ighg1* promoter.

(B) Genomic PCR analysis to confirm the insertion of *Hist1h3c* S87N mutant vector in the tail DNA of H3S87N KI. WT, wild-type; PC, positive control; NC, negative control.

(C) Sequence chromatography of TA cloning vector of Hist1h3c exon1 in GCB cells of spleen of H3S87N KI. The upper panel shows wild type (WT) and the lower panel shows H3S87N (c.G>A260) mutation.

(D) HE-stained sections of spleen tissues from H3S87N KI and WT. Splenic follicles are indicated by yellow dotted lines.

(E) Proportion of follicle area in spleen tissue from mice of the indicated genotypes at 15 weeks of age. The area of follicles was compared by 10 sections per 2 μm of spleen of one H3S87N KI and one WT.

(F) Spleen weights of mice at 15 weeks of age. Sp, spleen.

(G) The proportions of GCB, $Cd23^{high}Cd21^{dull}$ (FOB), $Cd23^{dull}Cd21^{high}$ (MZB) cells using flow cytometry at 15 weeks of age.

(H) Histograms showing cell surface Cd40 expression in GCB cells of spleen from H3S87N KI and WT.

Supplemental Figure 10

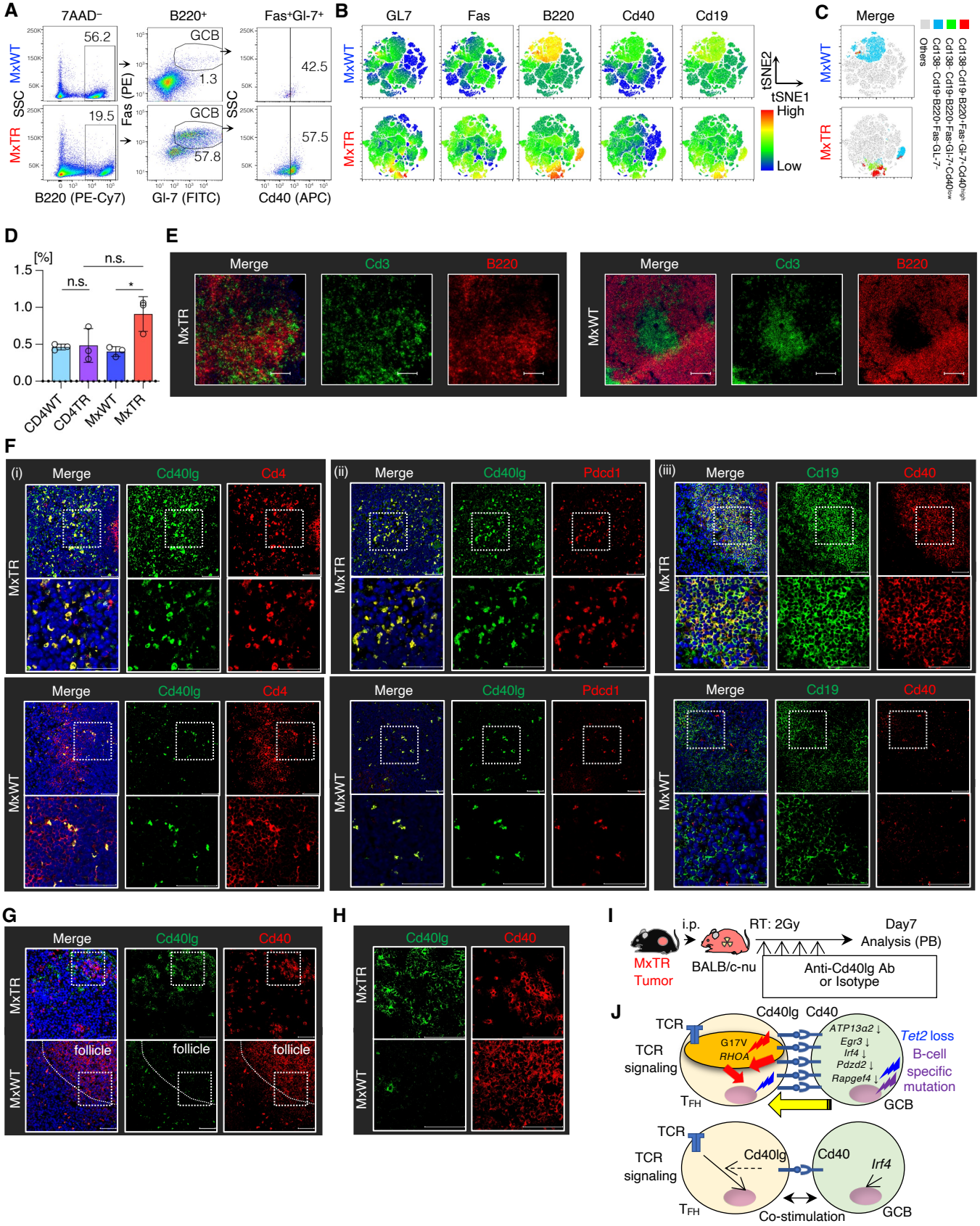

Supplemental Figure 10. Cd40 expression in GCB cells and treatment of mice with an anti-Cd40lg antibody

Representative flow cytometric plots (**A**) and tSNE heatmaps (**B**) of Cd19, B220, Fas, Gl-7, and Cd40 in spleen cells from tumor-bearing MxTR and MxWT at ~50 weeks of age.

(C) tSNE plots manually gated and integrated $Cd138^{-}Cd19^{+}B220^{+}Fas^{+}Gl\text{-}7^{+}Cd40^{high}$ (red), $Cd138^{-}Cd19^{+}B220^{+}Fas^{+}Gl\text{-}7^{+}Cd40^{low}$ (light green), $Cd138^{-}Cd19^{+}Fas^{-}Gl\text{-}7^{-}$ (light blue), and others (grey) using data from supplemental Figure. 9B.

(D) Cd40 expression in GCB cells at 20 weeks of age.

Immunofluorescence staining of spleen tissue in tumor-bearing MxTR or MxWT. (E) Green, Cd3; red, B220; blue, DAPI. Images were acquired at ×20. Scale bars, 100 μm. (F) (i) Green, Cd40lg; red, Cd4; blue, DAPI; (ii) green, Cd40lg; red, Pdcd1; blue, DAPI; (iii) green, Cd19; red, Cd40; blue, DAPI. Low (×40, top) and high (×100, bottom) magnification. High magnification image at bottom corresponds to dashed boxed area at upper. Scale bars, 50 μm.

(G, H) Green, Cd40lg; red, Cd40; blue, DAPI. High magnification image corresponds to dashed boxed area. Images were acquired at ×40 (G) or ×100 (H). Sp, Spleen. Scale bars, 50 μm.

(I) Experimental schema illustrating the treatment of tumor-bearing mice with an anti-mouse

Cd40lg (C154) antibody or control hamster IgGf (ab') isotype. To establish tumors, a single cell suspension prepared from tumors of MxTR was intraperitoneally injected into nude mice. i.p., intraperitoneal injection; RT, irradiation therapy; PB, peripheral blood; Ab, antibody.

(J) Schema showing the proposed interaction between T_{FH}-tumor and GCB cells in T_{FH}-like lymphomas (top panel) and physiological interaction between T_{FH} and GCB cells in normal follicles (bottom panel). TCR, T-cell receptor.

Supplemental Figure 11

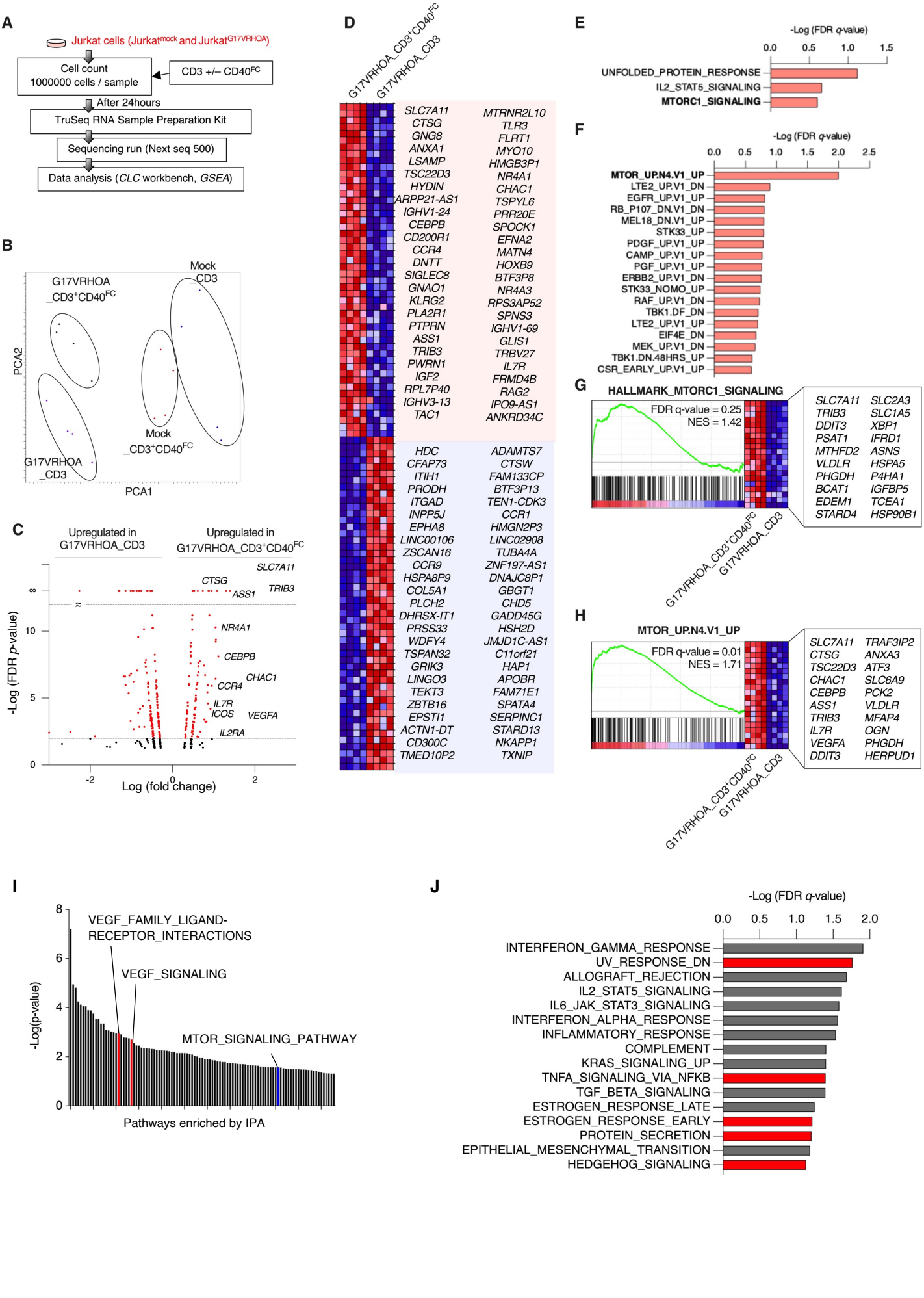

Supplemental Figure 11. RNA-seq analysis of Jurkat^{G17VRHOA} and Jurkat^{mock} with or without CD40-Fc chimera protein under the stimulation by an anti-CD3 antibody

(A) Overview of RNA-seq for Jurkat^{G17VRHOA} and Jurkat^{mock} with or without CD40-Fc chimera protein (CD40^{FC}) or Fc protein as control under the stimulation by an anti-CD3 antibody (CD3).

(B) PCA plot for RNA-seq.

(C) Volcano plot of up- or down-regulated genes in Jurkat^{G17VRHOA} with CD40-Fc chimera protein (G17VRHOA_CD3^{+}CD40^{FC}) or Fc protein as control (G17VRHOA_CD3) under the stimulation by an anti-CD3 antibody. Genes statistically different between two groups were shown in red at cut-off FDR p-value < 0.05.

(D) Heatmap by top 50 genes differentially expressed between G17VRHOA_CD3^{+}CD40^{FC} and G17VRHOA_CD3.

Gene sets enriched in G17VRHOA_CD3^{+}CD40^{FC} relative to G17VRHOA_CD3 based on GSEA with hallmark (E) or C5 (F) gene sets of MsigDB.

GSEA of HALLMARK MTORC1 SIGNALING (G) and MTOR UP.N4.V1 (H) for Jurkat^{G17VRHOA}. G17VRHOA_CD3^{+}CD40^{FC} (n = 4); and G17VRHOA_CD3 (n = 4).

(I) Gene sets enriched in G17VRHOA_CD3^{+}CD40^{FC} relative to G17VRHOA_CD3 based on IPA (Ingenuity Pathway Analysis). The gene sets related to VEGF and mTOR

pathway are highlighted in red and blue,

(J) Gene sets enriched in G17VRHOA_CD3^{+}CD40^{FC} relative to Mock_CD3^{+}CD40^{FC} based on GSEA with hallmark gene sets of MsigDB. Red bars indicate signatures enriched only in G17V_CD3^{+}CD40^{FC} vs Mock_CD3^{+}CD40^{FC}, not enriched in G17V_CD3 vs Mock_CD3.

Supplemental Figure 12

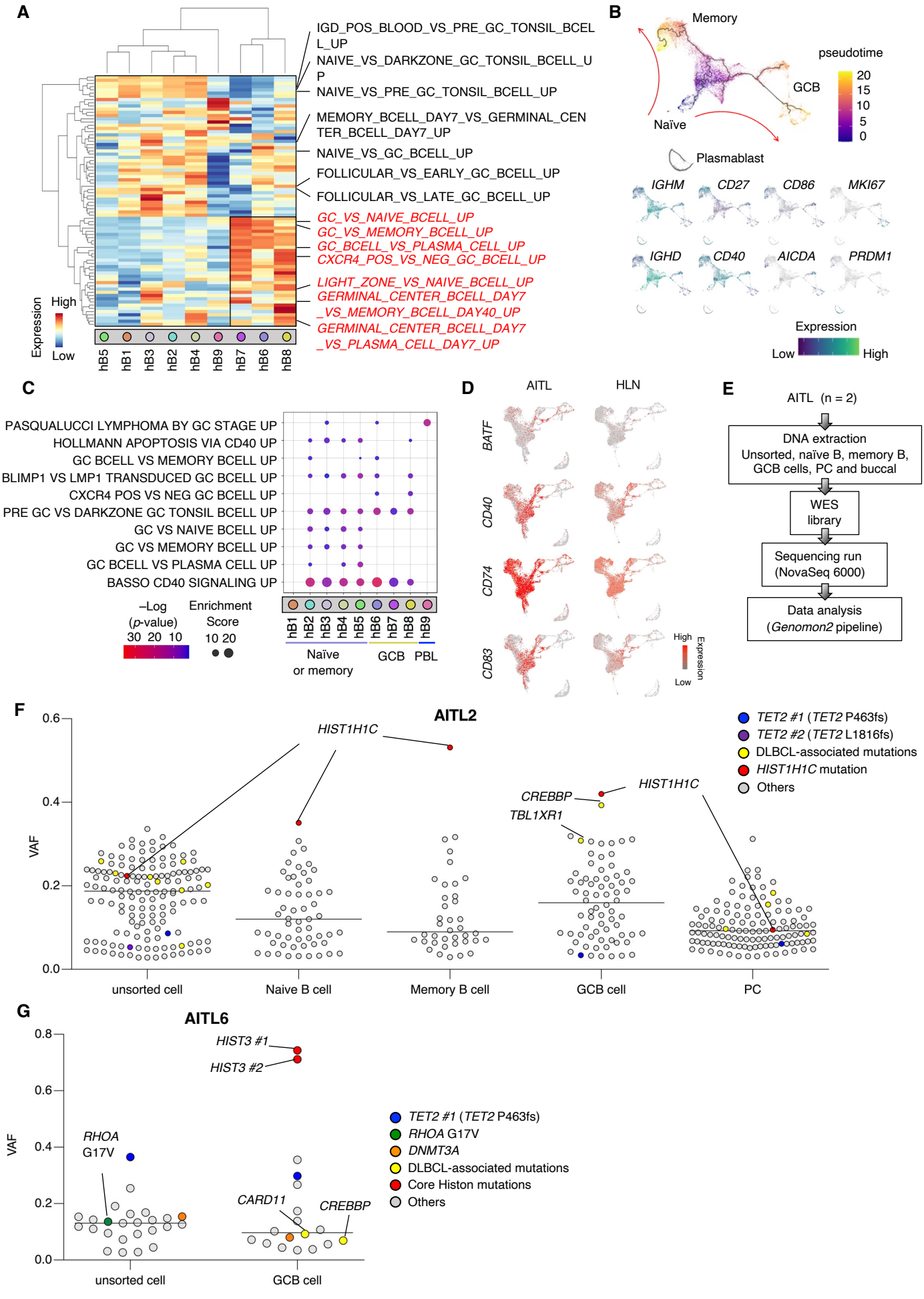

Supplemental Figure 12. Transcriptomic heterogeneity in B-cell subclusters of human AITL samples

(A) Heatmap showing pathways differentially enriched at hB1–9 based on GSVA with C7 genes of MsigDB. Gene sets in red indicate pathways enriched in the GCB clusters (hB6–8).

(B) scRNA-seq data of B-cell clusters sorted in silico from integrated data from AITL and HLN samples. Pseudo-time developmental stages (top) and feature plots for markers characteristic of B-cell differentiation (bottom). Dark winding lines in the UMAP indicate the estimated trajectory of the outbreak.

(C) Dot plots showing GCB-associated pathways detected by *Metascape* with the signature module set using upregulated gene lists in AITL compared to HLN. The dot size indicates the enrichment score. Cut-off, FDR p-value < 0.25.

(D) Feature plots of genes included in the AITL-B-specific gene set.

(E) Schema of WES for fractioned B and unsorted cells of AITL. GCB, germinal center B; PC, plasma cells.

Dot plots showing variant allele frequencies (VAF) for each mutation of unsorted cells or fractioned B cells of AITL2 (F) and AITL6 (G). VAF, variant allele frequency. Mutations in *TET2*, dark blue or purple; *RHOA* G17V, green; *DNMT3A*, orange; DLBCL-

associated mutations, yellow; *Histone* mutations, red; others, grey.

546 **REFERENCES**

547 1. Fujisawa M, Sakata-Yanagimoto M, Nishizawa S, et al. Activation of RHOA-VAV1
548 signaling in angioimmunoblastic T-cell lymphoma. *Leukemia*. 2018;32(3):694–702.

549 2. Nguyen TB, Sakata-Yanagimoto M, Fujisawa M, et al. Dasatinib Is an Effective
550 Treatment for Angioimmunoblastic T-cell Lymphoma. *Cancer Research*.
551 2020;80(9):1875–1884.

552 3. Lee PP, Fitzpatrick DR, Beard C, et al. A Critical Role for Dnmt1 and DNA Methylation
553 in T Cell Development, Function, and Survival. *Immunity*. 2001;15(5): 63-74.

554 4. Hudson WA, Li Q, Le C, Kersey JH. Xenotransplantation of human lymphoid
555 malignancies is optimized in mice with multiple immunologic defects. *Leukemia*.
556 1998;12(12):2029–2033.

557 5. Butler A, Hoffman P, Smibert P, Papalexi E, Satija R. Integrating single-cell transcriptomic
558 data across different conditions, technologies, and species. *Nature Biotechnology*. 2018;
559 36(5):411-420.

560 6. Hänzelmann S, Castelo R, Guinney J. GSVA: Gene set variation analysis for microarray
561 and RNA-Seq data. *BMC Bioinformatics*. 2013;14:7.

562 7. Zhao S, Guo Y, Sheng Q, Shyr Y. Heatmap3: an improved heatmap package with more
563 powerful and convenient features. *BMC Bioinformatics*. 2014;15(10):P16.

8. Efremova M, Vento-Tormo M, Teichmann SA, Vento-Tormo R. CellPhoneDB: inferring cell–cell communication from combined expression of multi-subunit ligand–receptor complexes. *Nature Protocols*. 2020;15(4):1484-1506.

9. Vento-Tormo R, Efremova M, Botting RA, et al. Single-cell reconstruction of the early maternal–fetal interface in humans. *Nature*. 2018; 563(7731):347-353

10. Dominguez PM, Ghamlouch H, Rosikiewicz W, et al. TET2 deficiency causes germinal center hyperplasia, impairs plasma cell differentiation and promotes B-cell lymphomagenesis. *Cancer Discovery*. 2018;CD-18-0657.

11. Reddy A, Zhang J, Davis NS, et al. Genetic and Functional Drivers of Diffuse Large B Cell Lymphoma. *Cell*. 2017;171(2):481-494.e15.

12. Robinson JT, Thorvaldsdóttir H, Winckler W, et al. Integrative genomics viewer. *Nature Biotechnology*. 2011;29(1): 24-6.

13. Bolotin DA, Poslavsky S, Mitrophanov I, et al. MiXCR: Software for comprehensive adaptive immunity profiling. *Nature Methods*. 2015;12(5):380-1.

14. Coffey D. LymphoSeq: Analyze high-throughput sequencing of T and B cell receptors. *R package version* 1.24.0.

15. Miura F, Enomoto Y, Dairiki R, Ito T. Amplification-free whole-genome bisulfite sequencing by post-bisulfite adaptor tagging. *Nucleic Acids Research*. 2012;40(17):.

16. Miura F, Shibata Y, Miura M, et al. Highly efficient single-stranded DNA ligation technique improves low-input whole-genome bisulfite sequencing by post-bisulfite adaptor tagging. *Nucleic Acids Research*. 2019;47(15):.

17. Jiang Y, Ortega-Molina A, Geng H, et al. *CREBBP* Inactivation Promotes the Development of HDAC3-Dependent Lymphomas. *Cancer Discovery*. 2017;7(1):38–53.